Application of the rescaling model at small Bjorken x values

A. V. Kotikov,[1,3] B. G. Shaikhatdenov,[3] and Pengming Zhang[1,2]
[1]*Institute of Modern Physics, Lanzhou 730000, China*
[2]*University of Chinese Academy of Sciences, Yuquanlu 19A, Beijing 100049, China*
[3]*Joint Institute for Nuclear Research, 141980 Dubna, Russia*
(Received 16 August 2017; published 5 December 2017)

The Bessel-inspired behavior of parton densities at small Bjorken x values, obtained in the case of the flat initial conditions for Dokshitzer-Gribov-Lipatov-Altarelli-Parisi evolution equations, is used along with "frozen" and analytic modifications of the strong coupling constant to study the so-called European Muon Collaboration effect. Among other results, this approach allowed predicting small x behavior of the gluon density in nuclei.

DOI: 10.1103/PhysRevD.96.114002

I. INTRODUCTION

The study of deep-inelastic scattering (DIS) of leptons off nuclei reveals an appearance of a significant nuclear effect (for a review see, e.g., [1,2]). It was first observed by the European Muon Collaboration [3] in the valence quark dominance region; hence the name. This observation rules out the naive picture of a nucleus as being a system of quasifree nucleons.

There in general are two mainstream approaches to studying the EMC effect. In the first one, which is at present more popular, nuclear parton distribution functions (nPDFs) are extracted from the global fits to nuclear data by using empirical parametrizations of their normalizations (see [4–6]). This is completely analogous to respective studies of usual (nucleon) PDFs (see recent analyses in [7]). Both PDFs and nPDFs are obtained from the numerical solution to Dokshitzer-Gribov-Lipatov-Altarelli-Parisi (DGLAP) equations [8].[1] The second strategy is based upon some models of nuclear PDFs (see different models in, for example, [11–14] and a recent review [15]).

Here we will follow the rescaling model [13,14], which was very popular some time ago. The model is based on a suggestion [16] that the effective confinement size of gluons and quarks in the nucleus is greater than in a free nucleon. In the framework of perturbative QCD it was found [13,14,16] that such a change in the confinement scale predicts that nPDFs and PDFs can be related by simply rescaling their arguments [see Eq. (8) below]. Thus, in a sense, the rescaling model lies in between the two above approaches: in its framework there are certain relations between usual and nuclear PDFs that result from shifting the values of kinematical variable μ^2; however, both densities obey DGLAP equations.

At that time, the model was established for the valence quark dominance region $0.2 \leq x \leq 0.8$. The aim of our paper is to extend its applicability to the region of small x values, where the rescaling values can be different for gluons and quarks. To see it clearly we use the generalized double-scaling approach (DAS) [17,18]. The latter is based upon the analytical solution to DGLAP equations in the small x region and generalizes earlier studies [19].

A few years ago most analyses of nPDFs have been done in the leading order (LO) of perturbation theory, but now the situation is drastically changed and the standard level of accuracy in current analyses is at the next-to-leading order (NLO) one (see [4,5]). Even more, there have already appeared a global analysis [6] performed at the next-to-next-to-leading order. Nevertheless the present analysis will be carried out in LO. We note that the analysis to this level of accuracy is just for the start and can be considered as a first step in our investigations in this direction. We are going to improve the accuracy at least to the NLO level in the future works.

II. SF F_2 AT LOW x

A reasonable agreement between HERA data [20] and predictions made by perturbative quantum chromodynamics (QCD) was observed for $Q^2 \geq 2\ \mathrm{GeV}^2$ [21], thereby promising that perturbative QCD is capable of describing the evolution of parton densities down to very low Q^2 values.

Some time ago ZEUS and H1 Collaborations have presented new precise combined data [22] on the structure function (SF) F_2. An application of the generalized DAS approach [18] at NLO shows that theoretical predictions are well compatible with experimental data at $Q^2 \geq 3 \div 4\ \mathrm{GeV}^2$ (see recent results in [23]).

In the present paper we perform a LO analysis of the combined data [22] where the SF F_2 has the following form

[1]Sometimes, in the analyses of DIS experimental data it is convenient to use an exact solution to DGLAP equations in the Mellin moment space and reconstruct SF F_2 from the moments (see recent paper [9] and references and discussions therein). The studies of nuclear effects in such a type of analysis can be found in [10], though its consideration is beyond the scope of the present study.

TABLE I. Values of the PDF fit parameters and χ_2 for three choices of the strong coupling constant (conventional, analytic and frozen), two choices of the number of active quark flavors (three and four) and a pair of Q^2 cuts.

$f = 3$ $Q^2 \geq$	$a_s(Q^2)$ 1 GeV^2	$a_s(Q^2)$ 3.5 GeV^2	$a_{an}(Q^2)$ 1 GeV^2	$a_{an}(Q^2)$ 3.5 GeV^2	$a_{fr}(Q^2)$ 1 GeV^2	$a_{fr}(Q^2)$ 3.5 GeV^2
A_g	0.46 ± 0.02	0.74 ± 0.04	1.16 ± 0.03	1.30 ± 0.04	0.96 ± 0.03	1.06 ± 0.04
A_q	1.58 ± 0.04	1.48 ± 0.06	1.16 ± 0.04	1.21 ± 0.07	1.23 ± 0.08	1.32 ± 0.07
Q_0^2	0.40 ± 0.01	0.46 ± 0.01	0.20 ± 0.01	0.16 ± 0.01	0.49 ± 0.01	0.53 ± 0.01
χ^2	365.7	69.7	149.7	42.9	140.4	47.6
$f = 4$ $Q^2 \geq$	$a_s(Q^2)$ 1 GeV^2	$a_s(Q^2)$ 3.5 GeV^2	$a_{an}(Q^2)$ 1 GeV^2	$a_{an}(Q^2)$ 3.5 GeV^2	$a_{fr}(Q^2)$ 1 GeV^2	$a_{fr}(Q^2)$ 3.5 GeV^2
A_g	0.47 ± 0.02	0.54 ± 0.03	0.65 ± 0.02	0.76 ± 0.03	0.96 ± 0.03	0.77 ± 0.03
A_q	1.58 ± 0.04	1.09 ± 0.06	0.95 ± 0.03	0.96 ± 0.04	1.23 ± 0.05	0.95 ± 0.06
Q_0^2	0.40 ± 0.01	0.37 ± 0.01	0.16 ± 0.01	0.19 ± 0.01	0.49 ± 0.01	0.43 ± 0.01
χ^2	366.0	57.0	166.3	43.6	140.0	40.6

$$F_2(x,\mu^2) = e f_q(x,\mu^2), \tag{1}$$

where $e = (\sum_1^f e_i^2)/f$ is an average of the squared quark charges. Notice that the approach used in these analyses will be analogous to that exploited in NLO ones carried out in [23–25].

The small-x asymptotic expressions for parton densities f_a can be written as follows

$$f_a(x,\mu^2) = f_a^+(x,\mu^2) + f_a^-(x,\mu^2), \quad (\text{hereafter } a = q, g)$$
$$f_g^+(x,\mu^2) = \left(A_g + \frac{4}{9}A_q\right)\tilde{I}_0(\sigma)e^{-\bar{d}_+ s} + O(\rho),$$
$$f_q^+(x,\mu^2) = \frac{f}{9}\left(A_g + \frac{4}{9}A_q\right)\rho\tilde{I}_1(\sigma)e^{-\bar{d}_+ s} + O(\rho), \tag{2}$$

$$f_g^-(x,\mu^2) = -\frac{4}{9}A_q e^{-d_- s} + O(x),$$
$$f_q^-(x,\mu^2) = A_q e^{-d_-(1)s} + O(x), \tag{3}$$

where I_ν ($\nu = 0, 1$) are the modified Bessel functions with

$$s = \ln\left(\frac{a_s(\mu_0^2)}{a_s(\mu^2)}\right), \qquad \sigma = 2\sqrt{|\hat{d}_+| s \ln\left(\frac{1}{x}\right)},$$
$$\rho = \frac{\sigma}{2\ln(1/x)},$$
$$a_s(\mu^2) \equiv \frac{\alpha_s(\mu^2)}{4\pi} = \frac{1}{\beta_0 \ln(\mu^2/\Lambda_{\rm LO}^2)} \tag{4}$$

and

$$\hat{d}_+ = -\frac{12}{\beta_0}, \quad \bar{d}_+ = 1 + \frac{20f}{27\beta_0}, \quad d_- = \frac{16f}{27\beta_0} \tag{5}$$

denote singular $\hat{d}_+$ and regular $\bar{d}_+$ parts of the "anomalous dimensions" $d_+(n)$ and $d_-(n)$,[2] respectively, in the limit $n \to 1$.

By using the expressions given above we have analyzed H1 and ZEUS data for F_2 [22]. In order to keep the analysis as simple as possible, here we take $\mu^2 = Q^2$ and $\alpha_s(M_Z^2) = 0.1168$ in agreement with ZEUS results presented in [20]. Moreover, we use the fixed flavor scheme with two different values $f = 3$ and $f = 4$ of active quarks.

As can be seen from Table I, the twist-two approximation looks reasonable for $Q^2 \geq 3.5$ GeV^2. It is almost completely compatible with NLO analyses done in [23–25]. Moreover, these results are rather close to original analyses (see [26] and references therein) performed by the HERAPDF group. As in the case of [26] our χ^2/DOF $\sim$ 1 unless combined H1 and ZEUS experimental data analyzed are kept according to $Q^2 \geq 3.5$ GeV^2.

At lower Q^2 there is certain disagreement, which is we believe to be explained by the higher-twist (HT) corrections playing their important role. These HT corrections have rather cumbersome form at low x [24]. As it was shown [25], it is very promising to use infrared modifications of the strong coupling constant in our analysis. Such types of coupling constants modify the low μ^2 behavior of parton densities and structure functions. What is important, they do not generate additional free parameters. Moreover, the present results will be applied in the analyses of NMC data (see Sec. V–VI) accumulated at very low Q^2 values, where the HT expansion ($\sim 1/Q^{2n}$) is thought to be not applicable.

So, following [25], we are going to use the so-called "frozen" $a_{\rm fr}(\mu^2)$ [27] and analytic $a_{\rm an}(\mu^2)$ [28] versions

[2]Note that the variables $d_\pm(n)$ are ratios $\gamma_\pm^{(\rm LO)}(n)/(2\beta_0)$ of LO anomalous dimensions $\gamma_\pm^{(\rm LO)}(n)$ and LO coefficient β_0 of QCD β-function.

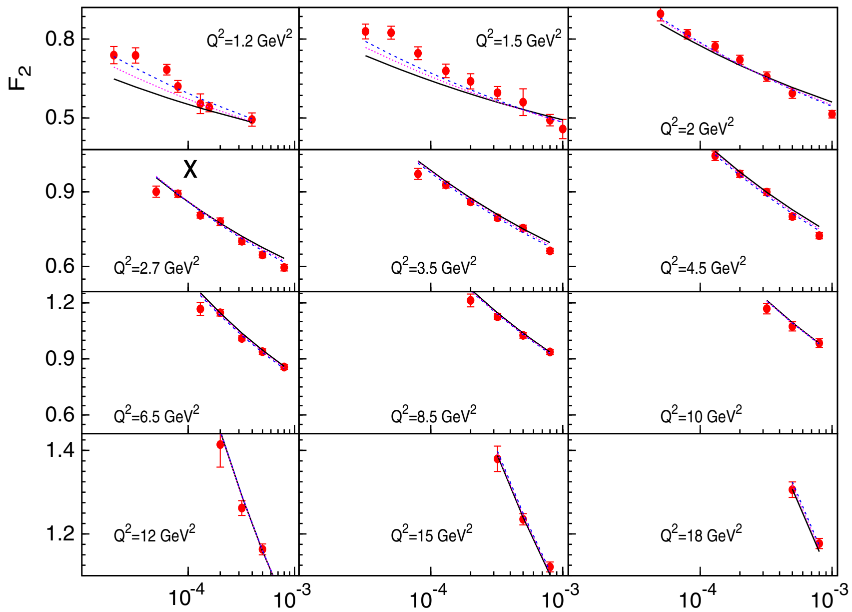

FIG. 1. x dependence of $F_2(x,Q^2)$ in bins of Q^2. The combined experimental data from H1 and ZEUS Collaborations [22] are compared with the LO fits for $Q^2 \geq 1$ GeV^2 implemented with a standard strong coupling constant (solid lines), and its frozen (dash-dotted lines) and analytic (dashed lines) modifications.

$$a_{\mathrm{fr}}(\mu^2) = a_s(\mu^2 + M_g^2),$$
$$a_{\mathrm{an}}(\mu^2) = a_s(\mu^2) - \frac{1}{\beta_0}\frac{\Lambda_{\mathrm{LO}}^2}{\mu^2 - \Lambda_{\mathrm{LO}}^2}, \tag{6}$$

where M_g is a gluon mass with $M_g = 1$ GeV^2 (see [29] and references therein[3]).

It is seen that the results of the fits carried out when $a_{\mathrm{fr}}(\mu^2)$ and $a_{\mathrm{an}}(\mu^2)$ are used, are very similar to the corresponding ones obtained in [23]. Moreover, note that the fits in the cases with frozen and analytic strong coupling constants look very much alike (see also [25,31]) and describe fairly well the data in the low Q^2 region, as opposed to the fits with a standard coupling constant, which largely fails here. The results are presented in Table I. With the number of active quarks $f = 4$, they are shown also in Fig. 1.

Just like the previous analyses [23,25,31] we observe strong improvement in the agreement between theoretical predictions and experimental data once frozen and analytic modifications to the coupling constant are applied. When the data are cut by $Q^2 \geq 1$ GeV^2, χ^2 value drops by more than two times. Ditto for the analyses of data with $Q^2 \geq 3.5$ GeV^2 imposed.

Recent NLO analyses (see the third paper in [23]) have been carried out within the framework of the fixed flavor scheme with $f = 3$ active light flavors and with a purely perturbative charm quark generated in a photon-gluon fusion (PGF) process. Such type of analyses for the complete SF $F_2(x,Q^2)$ cannot be done at LO.[4]

Therefore, we should use some fixed values of active quarks. Nevertheless, we would like to note that the results obtained here and those in [23–25], where various schemes were used, are very stable and close to each other.

III. RESCALING MODEL

In the rescaling model [14] SF F_2 and, therefore, valence part of quark densities, gets modified in the case of a nucleus A at intermediate and large x values $(0.2 \leq x \leq 0.9)$ as follows

$$F_2^A(x,\mu^2) = F_2(x,\mu_{A,v}^2), \quad f_{NS}^A(x,\mu^2) = f_{NS}(x,\mu_{A,v}^2), \tag{7}$$

where a new scale $\mu_{A,v}^2$ is related with μ^2 as

$$\mu_{A,v}^2 = \xi_v^A(\mu^2)\mu^2, \qquad \xi_v^A(\mu^2) = \left(\frac{\lambda_A^2}{\lambda_N^2}\right)^{a_s(\tilde{\mu}^2)/a_s(\mu^2)} \tag{8}$$

where some additional scale $\tilde{\mu}^2 = 0.66$ GeV^2, which was in its turn an initial point in a μ^2-evolution performed in [14]; it is then estimated in Appendix A of that paper. The quantity λ_A/λ_N stands for the ratio of quark confinement radii in a nucleus A and nucleon. The values of λ_A/λ_N and $\xi_v^A(\mu^2)$ at

[3]There are a number of various approaches to define the value of this gluon mass and even the form of its momentum dependence (see, e.g., a recent review [30]).

[4]Notice that the SF $F_{2c}(x,Q^2)$, the charm part of $F_2(x,Q^2)$, appears with $a_s(Q^2)$ and can be confronted already at LO with the data produced in a PGF process (see Sec. VII below).

TABLE II. δ_v and $\delta_\pm$ parameter values along with respective χ_2 obtained for different nuclei in the fits with analytic and frozen coupling constants. Here N stands for a number of experimental points.

A	^{2}D	^{4}He	^{7}Li	^{12}C	^{40}Ca
N		11	16	16	11
δ_v^A	0.01	0.06	0.05	0.08	0.11
δ_v^{AD}	0	0.05	0.04	0.07	0.10
$-\delta_{+,an}^{AD}$	0	0.06 ± 0.01	0.06 ± 0.01	0.11 ± 0.01	0.19 ± 0.01
$-\delta_{-,an}^{AD}$	0	0.24 ± 0.08	0.22 ± 0.07	0.41 ± 0.04	0.51 ± 0.04
χ^2_{an}	0	4.68	17	9.68	12
$-\delta_{+,fr}^{AD}$	0	0.06 ± 0.01	0.06 ± 0.01	0.12 ± 0.01	0.21 ± 0.02
$-\delta_{-,fr}^{AD}$	0	0.32 ± 0.08	0.28 ± 0.07	0.54 ± 0.04	0.71 ± 0.04
χ^2_{fr}	0	5	35	26	37

$\mu^2 = 20\ \mathrm{GeV}^2$ were evaluated for different nuclei and presented in Tables I and II in [14].

Since the factor $\xi_v^A(\mu^2)$ is μ^2 dependent, it is convenient to transform it to some μ^2 independent one. To this end, we consider the variable $\ln(\mu^2_{A,v}/\Lambda^2)$, which has the following form [from Eq. (8)]

$$\ln\left(\frac{\mu^2_{A,v}}{\Lambda^2}\right) = \ln\left(\frac{\mu^2}{\Lambda^2}\right) \cdot (1+\delta_v^A) \tag{9}$$

where the nuclear correction factor δ_v^A becomes μ^2 independent:

$$\delta_v^A = \frac{1}{\ln(\tilde{\mu}^2/\Lambda^2)} \ln\left(\frac{\lambda_A^2}{\lambda_N^2}\right), \tag{10}$$

where it is seen that two parameters, namely, the scale $\tilde{\mu}$ and ratio λ_A/λ_N, are combined to form a Q^2-independent quantity. Using Eqs. (9) and/or (10), we can recover results for δ_v^A, which are presented in Table II.

Since our parton densities contain the variable s defined in Eq. (4), it is convenient to consider its A modification. It has the following simple form:

$$s_v^A \equiv \ln\left(\frac{\ln(\mu^2_{A,v}/\Lambda^2)}{\ln(\mu_0^2/\Lambda^2)}\right) = s + \ln(1+\delta_v^A) \approx s + \delta_v^A, \tag{11}$$

i.e., the nuclear modification of the basic variable s depends on the μ^2 independent parameter δ_v^A, which possesses very small values.

IV. RESCALING MODEL AT LOW x

Standard evidence coming from earlier studies contains conclusion about inapplicability of the rescaling model at small x values (see, for example, [32]). It looks like it can be related with some simplifications of low x analyses (see, for example, [33], where the rise in EMC ratio was wrongly predicted at small x values).

Using an accurate study of DGLAP equations at low x within the framework of the generalized DAS approach, it is possible to achieve nice agreement with the experimental data for the DIS structure function F_2 (see previous section).[5] Therefore, we believe that all these indicate toward success in describing the EMC ratio by using the same approach.

We note that the main difference between global fits and DAS approach is in the restriction of applicability of the latter by low x region only, while the advantage of the DAS approach lies in the analytic solution to DGLAP equations.

Thus, we are trying to apply the DAS approach to low x region of EMC effect using a simple fact that the rise of parton densities increases with increasing Q^2 values. This way, with scales of PDF evolutions less than Q^2 (i.e., $\mu^2 \le Q^2$) in nuclear cases, we can directly reproduce the shadowing effect which is observed in the global fits. Since there are two components (2) for each parton density, we have two free parameters $\mu_\pm$ to be fit in the analyses of experimental data for EMC effect at low x values.

An application of the rescaling model at low x can be incorporated at LO as follows:

$$\begin{aligned} &F_2^A(x,\mu^2) = e f_q^A(x,\mu^2), \qquad F_2^N(x,\mu^2) = e f_q(x,\mu^2),\\ &f_a^A(x,\mu^2) = f_a^{A,+}(x,\mu^2) + f_a^{A,-}(x,\mu^2), \qquad (a=q,g),\\ &f_a^{A,\pm}(x,\mu^2) = f_a^{\pm}(x,\mu^2_{A,\pm}), \end{aligned} \tag{12}$$

with a similar definition of $\mu^2_{A,\pm}$ as in the previous section (up to replacement $v \to \pm$). The expressions for $f_a^\pm(x,\mu^2)$ are given in Eqs. (2) and (3).

Then, the corresponding values of $s_\pm^A$ are found to be

$$s_\pm^A \equiv \ln\left(\frac{\ln(\mu^2_{A,\pm}/\Lambda^2)}{\ln(\mu_0^2/\Lambda^2)}\right) = s + \ln(1+\delta_\pm^A), \tag{13}$$

[5] Moreover, using an analogous approach, good agreement was also found with the corresponding data for jet multiplicities [34].

because of the saturation at low x values for all considered Q^2 values, which in our case should be related with decreasing the arguments of "±" component. Therefore, the values of $\delta_\pm^A$ should be negative.

V. ANALYSIS OF THE LOW x DATA FOR NUCLEUS

Note that it is usually convenient to study the following ratio (see Fig. 1 in Ref. [15])

$$R_{F2}^{AD}(x,\mu^2) = \frac{F_2^A(x,\mu^2)}{F_2^D(x,\mu^2)}. \tag{14}$$

Using the fact that the nuclear effect in a deutron is very small (see Table I for the values of δ_v^A and discussions in [15]),[6] we can suggest that

$$\begin{aligned} &F_2^D(x,\mu^2) = ef_q(x,\mu^2), \qquad F_2^A(x,\mu^2) = e\bar{f}_q^A(x,\mu^2),\\ &\bar{f}_a^A(x,\mu^2) = \bar{f}_a^{A,+}(x,\mu^2) + \bar{f}_a^{A,-}(x,\mu^2), \qquad (a=q,g),\\ &\bar{f}_a^{A,\pm}(x,\mu^2) = f_a^\pm(x,\mu_{AD,\pm}^2), \end{aligned} \tag{15}$$

i.e.,

$$\begin{aligned} \bar{f}_g^{A,+}(x,\mu^2) &= \left(A_g + \frac{4}{9}A_q\right) I_0(\sigma_+^{AD}) e^{-\bar{d}_+ s_+^{AD}} + O(\rho_+^{AD}),\\ \bar{f}_q^{A,+}(x,\mu^2) &= \frac{f}{9}\left(A_g + \frac{4}{9}A_q\right)\rho_+^{AD} I_1(\sigma_+^{AD}) e^{-\bar{d}_+ s_+^{AD}} + O(\rho_+^{AD}), \end{aligned} \tag{16}$$

$$\begin{aligned} \bar{f}_g^{A,-}(x,\mu^2) &= -\frac{4}{9}A_q e^{-d_- s_-^{AD}} + O(x),\\ \bar{f}_q^{A,-}(x,\mu^2) &= A_q e^{-d_-(1) s_-^{AD}} + O(x), \end{aligned} \tag{17}$$

where

$$\begin{aligned} &\sigma_+^{AD} = \sigma(s \to s_+^{AD}), \qquad \rho_+^{AD} = \rho(s \to s_+^{AD}),\\ &s_\pm^{AD} \equiv \ln\left(\frac{\ln(\mu_{AD,\pm}^2/\Lambda^2)}{\ln(\mu_0^2/\Lambda^2)}\right) = s + \ln\left(1 + \delta_\pm^{AD}\right). \end{aligned} \tag{18}$$

We obtain the values of δ_+^{AD} and δ_-^{AD} by fitting NMC experimental data [36] for the EMC ratio at low x in the case of different nuclei. Since the experimental data for lithium and carbon are most precise and contain the maximal number of points (16 points for each nucleus), we perform combined fits of these data. Obtained results (with $\chi^2_{an} = 27$ and $\chi^2_{fr} = 43$ for 32 points) are presented in Table III and shown in Fig. 2.

[6]The study of nuclear effects in a deuteron can be found in [35], which also contains short reviews of preliminary investigations.

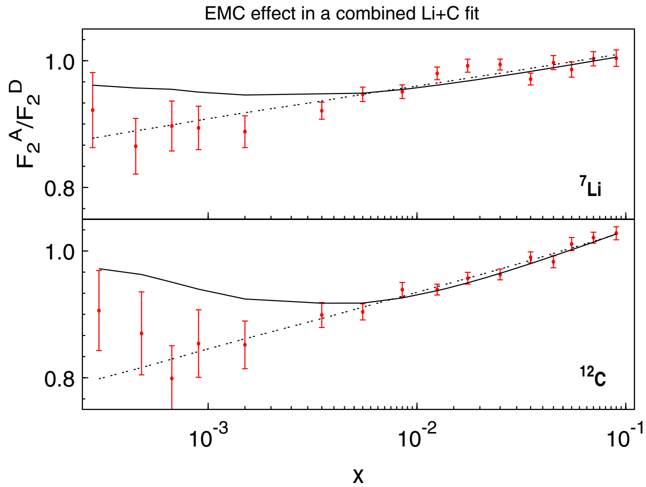

FIG. 2. small x dependence of $R_a^{AD}(x,\mu^2)$ for lithium and carbon. The combined experimental data from NMC [36] are fitted by LO expressions implemented with the frozen (solid lines) and analytic (dashed lines) modifications of the strong coupling constant.

As can be seen in Fig. 2 there is large difference between the fits with "frozen" and analytic versions of the strong couling constant. This is in contrast with the analysis done in Sec. I and results done in the earlier papers [31]. It seems that this difference comes about because we include in the analysis the region of very low Q^2 values, where frozen and analytic strong coupling constants are observed to be rather different (see also [29]).

VI. A DEPENDENCE AT LOW x

Taking NMC experimental data [36] along with E665 and HERMES Collaborations [37] for the EMC ratio at low x in the case of different nuclei, we can find the A dependence of $\delta_\pm^{AD}$, which can be parametrized as follows

$$-\delta_\pm^{AD} = c_\pm^{(1)} + c_\pm^{(2)} A^{1/3}. \tag{19}$$

As it was already mentioned in the previous section, usage of the analytic coupling constant leads to the fits with smaller χ^2 values. For example, the values of $c_\pm^{(1)}$ and $c_\pm^{(2)}$ found in the combined fit of the data (76 points) when the analytic coupling constant is used (with $\chi^2 = 89$) look like

$$\begin{aligned} &c_{+,an}^{(1)} = -0.055 \pm 0.015, \qquad c_{+,an}^{(2)} = 0.068 \pm 0.006,\\ &c_{-,an}^{(1)} = 0.071 \pm 0.101, \qquad c_{-,an}^{(2)} = 0.120 \pm 0.039. \end{aligned} \tag{20}$$

Now, using the A dependence (19), $R_{F2}^{AD}(x,\mu^2)$ values for any nucleus A can be predicted. What is more, we can consider also the ratios $R_a^{AD}(x,\mu^2)$ of parton densities in a nucleus and deuteron themselves,

TABLE III. $\delta_\pm$ parameter values obtained in the combined fit of lithium and carbon NMC datasets with analytic and frozen coupling constants.

	$-\delta^{AD}_{+,an}$	$-\delta^{AD}_{-,an}$	$-\delta^{AD}_{+,fr}$	$-\delta^{AD}_{-,fr}$
^{7}Li	0.061 ± 0.006	0.216 ± 0.065	0.073 ± 0.012	0.348 ± 0.067
^{12}C	0.105 ± 0.007	0.411 ± 0.042	0.139 ± 0.013	0.590 ± 0.041

$$R^{AD}_a(x,\mu^2) = \frac{\bar{f}^A_a(x,\mu^2)}{f_a(x,\mu^2)}, \qquad (a = q, g), \tag{21}$$

with $\bar{f}^A_a(x,\mu^2)$ and $f_a(x,\mu^2)$ defined in Eqs. (15)–(19) and (2)–(5), respectively.

Indeed, at LO $R^{AD}_q(x,\mu^2) = R^{AD}_{F2}(x,\mu^2)$; therefore, results for $R^{AD}_q(x,\mu^2)$ are already known. Since all the parameters of PDFs found within the framework of the generalized DAS approach are now fixed we can predict the ratio $R^{AD}_g(x,\mu^2)$ of the gluon densities in a nucleus and nucleon given in Eqs. (2), (3), (16), and (17), which is currently under intensive studies (see a recent paper [38] and review [39] along with references and discussion therein).

The results for $R^{AD}_{F2}(x,\mu^2)$ and $R^{AD}_g(x,\mu^2)$, depicted in Fig. 3, show some difference between these ratios. It is also seen that the difference is similar to that obtained in a recent EPPS16 analysis (see the first paper in [5])[7] However, what for $R^{AD}_{F2}(x,\mu^2)$ and $R^{AD}_g(x,\mu^2)$ themselves (irrespective of other results), we obtain a bit stronger effect at lowest x values, which does in fact not contradict the experimental data collected by the LHCb experiment (see recent review in [40]). Such a strong effect is also well compatible with the leading order EPPS09 analysis (which can also be found in [40]). It will be interesting to delve into more in-depth studies of the ratio $R^{AD}_g(x,\mu^2)$, which is one of our aims in the future.

VII. SF F_{2c} AT LOW x

Several years ago H1 [41] and ZEUS [42] Collaborations at HERA have separately presented their new data on the charm structure function F_{2c}[8] and more recently they have combined these data on $F_{2c}(x,\mu^2)$ [44]. The SF F_{2c} was found to be around 25% of F_2, which is considerably larger than what was observed by the European Muon Collaboration (EMC) at CERN [45] at larger x values, where it was only around 1% of F_2.

Ensuing and very extensive theoretical analyses were carried out to establish that the F_{2c} data can be described through the perturbative generation of charm in QCD [46]. In view of this, a PGF process in experiments with nucleon and nucleus targets is one of the most effective and promising studies of gluon density (see a recent review [47]).

Following [48] the SF F_{2c} at low x can be represented in the framework of the generalized DAS approach as follows

$$\begin{aligned} F_{2c}(x,\mu^2) &= e_c^2 a_s(\mu_c) C_{2,g}(1, z_c(\mu^2)) f_g(x,\mu^2), \\ z_c(\mu^2) &= \frac{m_c^2(\mu^2)}{\mu^2}, \qquad e_c = \frac{2}{3}, \end{aligned} \tag{22}$$

where $C_{2,g}(1, z_c(\mu^2))$ is a first Mellin moment of the LO PGF coefficient function $\tilde{C}_{2,g}(x, z_c(\mu^2))$. It can be obtained from the QED case [49] by adjusting the coupling constants (see also the direct calculations in [50,51]). The Mellin moment $C_{2,g}(1, z_c(\mu^2))$ has a very compact form [48]:

$$C_{2,g}(1,z) = \frac{2}{3}\left[1 - \frac{2(1-z)}{\sqrt{1+4z}} \ln \frac{\sqrt{1+4z}-1}{\sqrt{1+4z}+1}\right]. \tag{23}$$

The gluon density $f_g(x,\mu^2)$ is determined in (2) and (3).

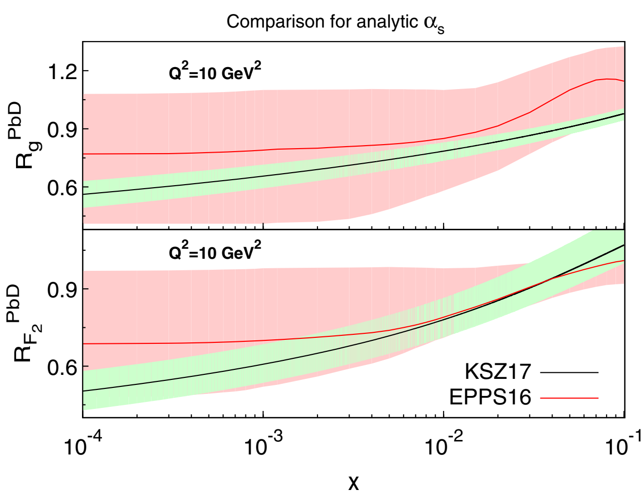

FIG. 3. x dependence of $R^{AD}_{F2}(x,\mu^2)$ and $R^{AD}_g(x,\mu^2)$ at $\mu^2 = 10$ GeV^2 for lead data. A green line with pink band (shows 90% uncertainties) is taken from the second paper of [39], while a black one with light green band is obtained in the present paper.

[7]Note that the result for $R^{AD}_g(x,\mu^2)$ along with its uncertainty is completely determined by both the rescaling model and the analytic form for parton densities at low x values we have used. Therefore, it is clear that the light green band for $R^{AD}_g(x,\mu^2)$ should become broader due to a freedom in using various models. Also note that a comparison between two uncertainty bands shown in Fig. 3 is in some sense misleading. The pink band is much broader since the EPPS16 global analysis included a fit to all available data across quite a wide range in x as opposed to small x consideration adopted in the present paper. Nonetheless, we decided to quote it here just to give the reader an idea about the subject, at least qualitatively.

[8]Open charm production was also observed in the COMPASS fixed target experiment [43].

The scale μ_c in (22) is actually not fixed because the results for F_{2c} are at LO. There are two widespread scales, $\mu_c^2 = 4m_c^2$ [47,52] and $\mu_c^2 = 4m_c^2 + \mu^2$ [41,42,44,48]. We will use below both of them (see the next subsection).

In the framework of the rescaling model the SF $F_{2c}^A(x,\mu^2)$ for nucleus A can be represented as follows

$$F_{2c}^A(x,\mu^2) = e_c^2 \sum_{i=\pm} a_s(\mu_c(\mu_{A,i}^2)) C_{2,g}(1, z_c(\mu_{A,i}^2)) f_g^i(x,\mu_{A,i}^2), \tag{24}$$

where the scale $\mu_{A,i}^2$ looks like

$$\mu_{A,\pm}^2 = \Lambda^2 \left(\frac{\mu^2}{\Lambda^2}\right)^{1+\delta_\pm^A} = \mu^2 \left(\frac{\mu^2}{\Lambda^2}\right)^{\delta_\pm^A}, \tag{25}$$

as it follows from (7) with the replacement $v \to \pm$.

The results for the ratios $R_{F2}^A(x,\mu^2)$, $R_g^A(x,\mu^2)$ and

$$R_c^A(x,\mu^2) = \frac{F_{2c}^A(x,\mu^2)}{F_{2c}(x,\mu^2)} \tag{26}$$

should be rather similar. Moreover, they have similar x-dependences, as it will be shown in the following subsection.

A. Analysis of the low x data

To have as close a relation with analyses in Sec. V as possible, let us consider the ratio

$$R_c^{AD}(x,\mu^2) = \frac{F_{2c}^A(x,\mu^2)}{F_{2c}^D(x,\mu^2)}. \tag{27}$$

As in Sec. V, we will use the following expressions for the SFs

$$\begin{aligned} F_{2c}^D(x,\mu^2) &= e_c^2 a_s(\mu_c) C_{2,g}(1, a_c(\mu^2)) f_g(x,\mu^2), \\ F_{2c}^A(x,\mu^2) &= e_c^2 \sum_{i=\pm} a_s(\mu_c(\mu_{AD,i}^2)) C_{2,g}(1, z_c(\mu_{AD,i}^2)) \\ &\quad \times \bar{f}_g^{A,\pm}(x,\mu^2), \end{aligned} \tag{28}$$

where the gluon density $\bar{f}_a^{A,\pm}(x,\mu^2) = f_a^\pm(x,\mu_{AD,\pm}^2)$ is defined in (16) and (17). The scale $\mu_{AD,\pm}^2$ can be obtained from (25) with the replacement $\delta_\pm^A \to \delta_\pm^{AD}$, by analogy with analyses in Sec. V.

The results for the ratios $R_c^{AD}(x,\mu^2)$,

$$R_{cg}^{AD}(x,\mu^2) = \frac{R_c^{AD}(x,\mu^2)}{R_g^{AD}(x,\mu^2)} \quad \text{and} \quad R_{c2}^{AD}(x,\mu^2) = \frac{R_c^{AD}(x,\mu^2)}{R_{F2}^{AD}(x,\mu^2)} \tag{29}$$

are presented in Fig. 4 for $\mu^2 = 10\ \mathrm{GeV}^2$. Since the μ^2-dependence of m_c is not strong, we use fixed $m_c = 1.27$ GeV [53] in our analysis.

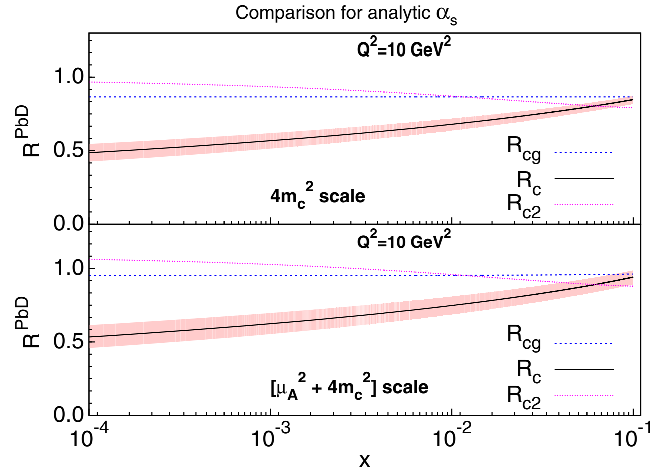

FIG. 4. x dependence of $R_c^{AD}(x,\mu^2)$, $R_{cg}^{AD}(x,\mu^2)$ and $R_{c2}^{AD}(x,\mu^2)$ at $\mu^2 = 10\ \mathrm{GeV}^2$ for lead data and two choices of μ_c scale: $\mu_c^2 = 4m_c^2$ and $\mu_c^2 = 4m_c^2 + \mu^2$ are shown by black, blue, and pink lines, respectively. A band represents 90% level uncertainties in determining $R_c^{AD}(x,\mu^2)$ values.

As can be seen in Fig. 4, results look very much the same for both scales of μ_c. What is more, a behavior of the ratio $R_c^{AD}(x,\mu^2)$ is a little bit weaker than that of $R_{F2}^{AD}(x,\mu^2)$ and a bit stronger than that observed for $R_g^{AD}(x,\mu^2)$. We hope that the x-dependence of the ratio $R_c^{AD}(x,\mu^2)$, along with that of $R_g^{AD}(x,\mu^2)$, can be measured at a future Electron–Ion Collider (see [47] and discussion therein).

VIII. CONCLUSION

Using a recent progress in the application of double-logarithmic approximations (see [18,23,34]) to the studies of small x behavior of the structure and fragmentation functions, respectively, we applied the DAS approach [17,18] to examine an EMC F_2 structure function ratio between various nuclei and a deutron. Within a framework of the rescaling model [14,16] good agreement between theoretical predictions and respective experimental data is achieved.

The theoretical formulas contain certain parameters, whose values were fit in the analyses of experimental data. Once the fits are carried out we have predictions for the corresponding ratios of parton densities without free parameters. These results were used to predict small x behavior of the gluon density in nuclei, which is at present poorly known.

The ratios $R_a^{AD}(x,\mu^2)$ $(a = q, g)$ predicted in the present paper are compatible with those given by various groups working in the area. From our point of view, it is quite valuable that the application of the rescaling model [14,16] provided us with very simple forms for these ratios. It should also be mentioned that without any free parameters we can predict the ratio $R_c^{AD}(x,\mu^2)$ of charm parts, $F_{2c}^A(x,\mu^2)$ and $F_{2c}^D(x,\mu^2)$, of the respective structure functions. This latter ratio has a simple form and it is very similar to the corresponding ratio of the complete structure functions $F_2^A(x,\mu^2)$ and $F_2^D(x,\mu^2)$.

Following [18,23] we plan to extend our analysis to the NLO level of approximation, the accuracy that is currently a standard in nPDF studies. Also, we are going to consider a rather broad range of the Bjorken variable x by using parametrizations of parton densities, which will be constructed by analogy with the one obtained earlier in the valence quark case (see [54]). The usage of such type of parametrizations will make it possible to carry out the present analysis of the data accumulated within the range of intermediate x values, which is presently under active considerations.

ACKNOWLEDGMENTS

Support by the National Natural Science Foundation of China (Grant No. 11575254) is acknowledged. A. V. K. and B. G. S. thank Institute of Modern Physics for invitation. A. V. K. is also grateful to the CAS President's International Fellowship Initiative (Grant No. 2017VMA0040) for support. The work of A. V. K. and B. G. S. was in part supported by the RFBR Foundation through the Grant No. 16-02-00790-a.

[1] M. Arneodo, Nuclear effects in structure functions, Phys. Rep. **240**, 301 (1994); P. R. Norton, The EMC effect, Rep. Prog. Phys. **66**, 1253 (2003).

[2] K. Rith, Present status of the EMC effect, Subnuclear series **51**, 431 (2015); S. Malace, D. Gaskell, D. W. Higinbotham, and I. Cloet, The challenge of the EMC effect: Existing data and future directions, Int. J. Mod. Phys. E **23**, 1430013 (2014); K. Kovarik *et al.*, nCTEQ15—Global analysis of nuclear parton distributions with uncertainties in the CTEQ framework, Phys. Rev. D **93**, 085037 (2016).

[3] J. J. Aubert *et al.* (European Muon Collaboration), The ratio of the nucleon structure functions $F2_n$ for iron and deuterium, Phys. Lett. **123B**, 275 (1983).

[4] K. J. Eskola, H. Paukkunen, and C. A. Salgado, EPS09: A new generation of NLO and LO nuclear parton distribution functions, J. High Energy Phys. 04 (2009) 065; M. Hirai, S. Kumano, and T.-H. Nagai, Determination of nuclear parton distribution functions and their uncertainties in next-to-leading order, Phys. Rev. C **76**, 065207 (2007); D. de Florian, R. Sassot, P. Zurita, and M. Stratmann, Global analysis of nuclear parton distributions, Phys. Rev. D **85**, 074028 (2012); K. Kovarik *et al.*, nCTEQ15—Global analysis of nuclear parton distributions with uncertainties in the CTEQ framework, Phys. Rev. D **93**, 085037 (2016).

[5] K. J. Eskola, P. Paakkinen, H. Paukkunen, and C. A. Salgado, EPPS16: Nuclear parton distributions with LHC data, Eur. Phys. J. C **77**, 163 (2017).

[6] H. Khanpour and S. Atashbar Tehrani, Global analysis of nuclear parton distribution functions and their uncertainties at next-to-next-to-leading order, Phys. Rev. D **93**, 014026 (2016).

[7] S. Dulat, T.-J. Hou, J. Gao, M. Guzzi, J. Huston, P. Nadolsky, J. Pumplin, C. Schmidt, D. Stump, and C.-P. Yuan, New parton distribution functions from a global analysis of quantum chromodynamics, Phys. Rev. D **93**, 033006 (2016); L. A. Harland-Lang, A. D. Martin, P. Motylinski, and R. S. Thorne, Parton distributions in the LHC era: MMHT 2014 PDFs, Eur. Phys. J. C **75**, 204 (2015); R. D. Ball *et al.* (NNPDF Collaboration), Parton distributions for the LHC Run II, J. High Energy Phys. 04 (2015) 040; A. Accardi *et al.*, A critical appraisal and evaluation of modern PDFs, Eur. Phys. J. C **76**, 471 (2016); Constraints on large-x parton distributions from new weak boson production and deep-inelastic scattering data, Phys. Rev. D **93**, 114017 (2016); P. Jimenez-Delgado and E. Reya, Delineating parton distributions and the strong coupling, Phys. Rev. D **89**, 074049 (2014); S. Alekhin, J. Blümlein, S. Moch, and R. Plačakytė, Parton distribution functions, α_s and heavy-quark masses for LHC Run II, Phys. Rev. D **96**, 014011 (2017).

[8] V. N. Gribov and L. N. Lipatov, Deep inelastic e p scattering in perturbation theory, Sov. J. Nucl. Phys. **15**, 438 (1972); $e+e-$ pair annihilation and deep inelastic e p scattering in perturbation theory, Sov. J. Nucl. Phys. **15**, 675 (1972); L. N. Lipatov, The parton model and perturbation theory, Sov. J. Nucl. Phys. **20**, 94 (1975); G. Altarelli and G. Parisi, Asymptotic freedom in parton language, Nucl. Phys. **B126**, 298 (1977); Y. L. Dokshitzer, Calculation of the structure functions for deep inelastic scattering and $e+e-$ annihilation by perturbation theory in quantum chromodynamics, Sov. Phys. JETP **46**, 641 (1977).

[9] A. V. Kotikov, V. G. Krivokhizhin, and B. G. Shaikhatdenov, Gottfried sum rule in QCD NS analysis of DIS fixed target data, arXiv:1612.06412.

[10] V. G. Krivokhizhin and A. V. Kotikov, A systematic study of QCD coupling constant from deep-inelastic measurements, Phys. At. Nucl. **68**, 1873 (2005); Functions of the nucleon structure and determination of the strong coupling constant, Phys. Part. Nucl. **40**, 1059 (2009).

[11] S. A. Kulagin and R. Petti, Global study of nuclear structure functions, Nucl. Phys. **A765**, 126 (2006); Nuclear parton distributions and the Drell-Yan process, Phys. Rev. C **90**, 045204 (2014).

[12] R. Wang, X. Chen, and Q. Fu, Global study of nuclear modifications on parton distribution functions, Nucl. Phys. **B920**, 1 (2017); R. Wang and X. Chen, Nuclear force and the EMC effect, Phys. Lett. B **743**, 267 (2015); X. Chen, J. Ruan, R. Wang, P. Zhang, and W. Zhu, Applications of a nonlinear evolution equation II: The EMC effect, Int. J. Mod. Phys. E **23**, 1450058 (2014); W. Zhu, R. Wang, and

J. Ruan, Looking for quark saturation in proton and nuclei, Int. J. Mod. Phys. E **26**, 1750009 (2017).

[13] R. L. Jaffe, F. E. Close, R. G. Roberts, and G. G. Ross, On the nuclear dependence of electroproduction, Phys. Lett. **134B**, 449 (1984); O. Nachtmann and H. J. Pirner, Color conductivity in nuclei and the Emc effect, Z. Phys. C **21**, 277 (1984).

[14] F. E. Close, R. L. Jaffe, R. G. Roberts, and G. G. Ross, Change of confinement scale in nuclei: Predictions for structure functions confront electroproduction data, Phys. Rev. D **31**, 1004 (1985).

[15] S. A. Kulagin, Nuclear parton distributions, Eur. Phys. J. Web Conf. **138**, 01006 (2017).

[16] F. E. Close, R. G. Roberts, and G. G. Ross, The effect of confinement size on nuclear structure functions, Phys. Lett. **129B**, 346 (1983); R. L. Jaffe, Quark Distributions in Nuclei, Phys. Rev. Lett. **50**, 228 (1983).

[17] L. Mankiewicz, A. Saalfeld, and T. Weigl, On the analytical approximation to the GLAP evolution at small x and moderate Q^2, Phys. Lett. B **393**, 175 (1997).

[18] A. V. Kotikov and G. Parente, Small x behavior of parton distributions with soft initial conditions, Nucl. Phys. **B549**, 242 (1999).

[19] A. De Rújula, S. L. Glashow, H. D. Politzer, S. B. Treiman, F. Wilczek, and A. Zee, Possible non-Regge behavior of electroproduction structure functions, Phys. Rev. D **10**, 1649 (1974); R. D. Ball and S. Forte, A direct test of perturbative QCD at small x, Phys. Lett. B **336**, 77 (1994).

[20] C. Adloff *et al.* (H1 Collaboration), Nucl. Phys. **B497**, 3 (1997); Deep-inelastic inclusive ep scattering at low x and a determination of α_s, Eur. Phys. J. C **21**, 33 (2001); S. Chekanov *et al.* (ZEUS Collaboration), Measurement of the neutral current cross section and F_2 structure function for deep inelastic e^+p scattering at HERA, Eur. Phys. J. C **21**, 443 (2001).

[21] A. M. Cooper-Sarkar, R. C. E. Devenish, and A. de roeck, Structure functions of the nucleon and their interpretation, Int. J. Mod. Phys. A **13**, 3385 (1998); A. V. Kotikov, Deep inelastic scattering: Q^2 dependence of structure functions, Phys. Part. Nucl. **38**, 1 (2007); Erratum, Phys. Part. Nucl. **38**, 828(E) (2007).

[22] F. D. Aaron *et al.* (H1 and ZEUS Collaboration), Combined measurement and QCD analysis of the inclusive $e^{\pm}$ p scattering cross sections at HERA, J. High Energy Phys. 01 (2010) 109.

[23] A. V. Kotikov and B. G. Shaikhatdenov, Q2-evolution of parton densities at small x values. Combined H1 and ZEUS F2 data, Phys. Part. Nucl. **44**, 543 (2013); Q^2 evolution of parton distributions at small values of x: Effective scale for combined H1 and ZEUS data on the structure function F_2, Phys. At. Nucl. **78**, 525 (2015); Q^2-evolution of parton densities at small x values. Charm contribution in the combined H1 and ZEUS F_2 data, Phys. Part. Nucl. **48**, 829 (2017).

[24] A. Yu. Illarionov, A. V. Kotikov, and G. Parente, Small x behavior of parton distributions: a study of higher twist effects, Phys. Part. Nucl. **39**, 307 (2008).

[25] G. Cvetic, A. Yu. Illarionov, B. A. Kniehl, and A. V. Kotikov, Small-x behavior of the structure function F_2 and its slope $\partial \ln F_2/\partial \ln(1/x)$ for "frozen" and analytic strong-coupling constants, Phys. Lett. B **679**, 350 (2009).

[26] A. M. Cooper-Sarkar *et al.*, Study of HERA data at low Q^2 and low x, *Proc. Sci.*, DIS2016 (2016) 013; I. Abt, A. M. Cooper-Sarkar, B. Foster, V. Myronenko, K. Wichmann, and M. Wing, Study of HERA ep data at low Q^2 and low x_{Bj} and the need for higher-twist corrections to standard perturbative QCD fits, Phys. Rev. D **94**, 034032 (2016); Z. Zhang (H1 and ZEUS Collaborations), HERA inclusive neutral and charged current cross sections and a new PDF fit, HERAPDF 2.0, Acta Phys. Pol. B Proc. Suppl. **8**, 957 (2015).

[27] B. Badelek, J. Kwiecinski, and A. Stasto, A model for $F(L)$ and $R = F(L)/F(T)$ at low x and low Q^2, Z. Phys. C **74**, 297 (1997); Y. A. Simonov, Asymptotic freedom and IR freezing in QCD: the role of gluon paramagnetism, Phys. At. Nucl. **74**, 1223 (2011).

[28] D. V. Shirkov and I. L. Solovtsov, Analytic Model for the QCD Running Coupling with Universal alpha-s (0) Value, Phys. Rev. Lett. **79**, 1209 (1997).

[29] D. V. Shirkov, 'Massive' perturbative QCD, regular in the IR limit, Phys. Part. Nucl. Lett. **10**, 186 (2013).

[30] A. Deur, S. J. Brodsky, and G. F. de Teramond, The QCD running coupling, Prog. Part. Nucl. Phys. **90**, 1 (2016).

[31] A. V. Kotikov, A. V. Lipatov, and N. P. Zotov, Longitudinal structure function F_L: Perturbative QCD and K_T-factorization versus experimental data at fixed W, J. Exp. Theor. Phys. **101**, 811 (2005); A. V. Kotikov, V. G. Krivokhizhin, and B. G. Shaikhatdenov, Analytic and 'frozen' QCD coupling constants up to NNLO from DIS data, Phys. At. Nucl. **75** (2012) 507.

[32] A. V. Efremov, On the nature of the Emc effect, Phys. Lett. **174B**, 219 (1986).

[33] A. V. Kotikov, The Emc ratio as a function of x, Q^2 in the rescaling model, Sov. J. Nucl. Phys. **50**, 127 (1989).

[34] P. Bolzoni, B. A. Kniehl, and A. V. Kotikov, Gluon and Quark Jet Multiplicities at $N^3LO + NNLL$, Phys. Rev. Lett. **109**, 242002 (2012); Average gluon and quark jet multiplicities at higher orders, Nucl. Phys. **B875**, 18 (2013); B. A. Kniehl and A. V. Kotikov, α_s from hadron multiplicities via SUSY-like relation between anomalous dimensions, arXiv:1702.03193.

[35] S. Alekhin, S. A. Kulagin, and R. Petti, Nuclear effects in the deuteron and constraints on the d/u ratio, Phys. Rev. D **96**, 054005 (2017).

[36] M. Arneodo *et al.* (New Muon Collaboration), The structure function ratios F2(li)/F2(D) and F2(C)/F2(D) at small x, Nucl. Phys. **B441**, 12 (1995); The A dependence of the nuclear structure function ratios, Nucl. Phys. **B481**, 3 (1996); P. Amaudruz *et al.* (New Muon Collaboration), A reevaluation of the nuclear structure function ratios for D, He, Li-6, C and Ca, Nucl. Phys. **B441**, 3 (1995).

[37] M. R. Adams *et al.* (E665 Collaboration), Shadowing in inelastic scattering of muons on carbon, calcium and lead at low x(Bj), Z. Phys. C **67**, 403 (1995); K. Ackerstaff *et al.* (HERMES Collaboration), Nuclear effects on $R = \sigma_L/\sigma_T$ in deep inelastic scattering, Phys. Lett. B **475**, 386 (2000); Erratum, Phys. Lett. B **567**, 339(E) (2003).

[38] L. Frankfurt, V. Guzey, and M. Strikman, Dynamical model of antishadowing of the nuclear gluon distribution, Phys. Rev. C **95**, 055208 (2017).

[39] N. Armesto, Nuclear shadowing, J. Phys. G **32**, R367 (2006); H. Paukkunen, Status of nuclear PDFs after the first LHC p-Pb run, Nucl. Phys. **A967**, 241 (2017).

[40] M. Winn, Heavy flavour production in proton-lead and lead-lead collisions with LHCb, Nucl. Phys. **A967**, 596 (2017).

[41] F. D. Aaron *et al.* (H1 Collaboration), Measurement of the $D^{\pm}$ meson production cross section and ${F_2}^{c\bar{c}}$, at high Q^2, in ep scattering at HERA, Phys. Lett. B **686**, 91 (2010); Measurement of the charm and beauty structure functions using the H1 vertex detector at HERA, Eur. Phys. J. C **65**, 89 (2010).

[42] S. Chekanov *et al.* (ZEUS Collaboration), Measurement of charm and beauty production in deep inelastic ep scattering from decays into muons at HERA, Eur. Phys. J. C **65**, 65 (2010); H. Abramowicz *et al.* (ZEUS Collaboration), Measurement of beauty and charm production in deep inelastic scattering at HERA and measurement of the beauty-quark mass, J. High Energy Phys. 09 (2014) 127.

[43] C. Adolph *et al.* (COMPASS Collaboration), Leading and next-to-leading order gluon polarization in the nucleon and longitudinal double spin asymmetries from open charm muoproduction, Phys. Rev. D **87**, 052018 (2013); D* and D meson production in muon nucleon interactions at 160 GeV/c, Eur. Phys. J. C **72**, 2253 (2012).

[44] H. Abramowicz *et al.* (H1 and ZEUS Collaborations), Combination and QCD analysis of charm production cross section measurements in deep-inelastic ep scattering at HERA, Eur. Phys. J. C **73**, 2311 (2013).

[45] J. J. Aubert *et al.* (European Muon Collaboration), Production of charmed particles in 250-GeV μ^+—iron interactions, Nucl. Phys. **B213**, 31 (1983); An experimental limit on the intrinsic charm component of the nucleon, Phys. Lett. **110B**, 73 (1982); A study of dimuon events in 280-GeV muon interactions, Phys. Lett. **94B**, 96 (1980).

[46] S. Frixione, M. L. Mangano, P. Nason, and G. Ridolfi, Total cross-sections for heavy flavor production at HERA, Phys. Lett. B **348**, 633 (1995); S. Frixione, P. Nason, and G. Ridolfi, Differential distributions for heavy flavor production at HERA, Nucl. Phys. **B454**, 3 (1995).

[47] E. Chudakov, D. Higinbotham, C. Hyde, S. Furletov, Y. Furletova, D. Nguyen, M. Stratmann, M. Strikman, and C. Weiss, Heavy quark production at an Electron-Ion Collider, J. Phys. Conf. Ser. **770**, 012042 (2016); Probing nuclear gluons with heavy quarks at EIC, *Proc. Sci.*, DIS2016 (2016) 143.

[48] A. Y. Illarionov, B. A. Kniehl, and A. V. Kotikov, Heavy-quark contributions to the ratio F(L)/F(2) at low x, Phys. Lett. B **663**, 66 (2008); A. Y. Illarionov and A. V. Kotikov, F_2^c at low x, Phys. At. Nucl. **75**, 1234 (2012).

[49] V. N. Baier, V. S. Fadin, and V. A. Khoze, Electromagnetic pair production, Yad. Fiz. **16**, 1051 (1972); V. G. Zima, Electron-positron pair production, Sov. Phys. JETP **23**, 104 (1966); V. M. Budnev, I. F. Ginzburg, G. V. Meledin, and V. G. Serbo, The two photon particle production mechanism. Physical problems. Applications. Equivalent photon approximation, Phys. Rep. **15**, 181 (1975).

[50] E. Witten, Heavy quark contributions to deep inelastic scattering, Nucl. Phys. **B104**, 445 (1976); J. P. Leveille and T. J. Weiler, Characteristics of heavy quark leptoproduction in QCD, Nucl. Phys. **B147**, 147 (1979); M. A. Shifman, A. I. Vainshtein, and V. I. Zakharov, Remarks on charm electroproduction in QCD, Nucl. Phys. **B136**, 157 (1978).

[51] A. V. Kotikov, A. V. Lipatov, G. Parente, and N. P. Zotov, The contribution of off-shell gluons to the structure functions ${F_2}^c$ and ${F_L}^c$ and the unintegrated gluon distributions, Eur. Phys. J. C **26**, 51 (2002).

[52] M. Gluck, E. Reya, and M. Stratmann, Heavy quarks at high-energy colliders, Nucl. Phys. **B422**, 37 (1994).

[53] C. Patrignani *et al.* (Particle Data Group), Review of particle physics, Chin. Phys. C **40**, 100001 (2016).

[54] A. Y. Illarionov, A. V. Kotikov, S. S. Parzycki, and D. V. Peshekhonov, New type of parametrizations for parton distributions, Phys. Rev. D **83**, 034014 (2011).